Electronic Supplementary Information

A Higher Voltage Fe(II) Bipyridine Complex for Non-Aqueous Redox Flow Batteries

Claudina X. Cammack,[a] Harry D. Pratt III,[a] Leo J. Small,[a] Travis M. Anderson[a]*

[a] Sandia National Laboratories, Albuquerque, New Mexico, 87185-0613, USA

*Email: tmander@sandia.gov

I. Synthesis

Ferrocenium tetrafluoroborate ($FcBF_4$) was prepared according to literature procedure.[1]

Synthesis of 1,1'-di(trifluoroborate)-2,2'-bipyridinium: bpy (1.34 g, 8.6 mmol) was dissolved in diethyl ether (10 mL) and flushed with N_2. The solution was cooled to 0 ºC, and $BF_3{\cdot}OEt_2$ was added dropwise with fast-stirring, turning the solution into a cloudy-white mixture. The reaction continued stirring while warming to room temperature overnight. The white precipitate was filtered and dried under vacuum (2.37 g, 94 %). ^{1}H NMR (500 MHz, DMSO-d_6): δ 8.83 (dd, J = 5.1, 2.2 Hz, 2H), 8.57 (d, J = 8.1 Hz, 2H), 8.27 (td, J = 7.8, 1.8 Hz, 2H), 7.75 (dd, J = 7.2, 5.5 Hz, 2H). ^{13}C (125 MHz, acetone-d_6): δ 147.70, 147.34, 144.64, 128.56, 124.47. HRMS: Calcd. for $C_{10}H_8BF_3N_2$ [M^+] m/z 224.0847, found 224.0763.

II. Preparation of post-battery samples for characterization:

Post-battery cyclic voltammogram solutions were prepared by diluting the catholyte and anolyte samples (assembled as 0.2 M) in the respective 0.5 M supporting electrolyte down to 10 mM: 100 µL catholyte/anolyte and 1.9 mL supporting electrolyte.

UV-Vis spectroscopy solutions on post-battery samples were prepared by diluting 0.2 µL in 3 mL of 0.5 M $TEABF_4$ in propylene carbonate to determine post-cycling concentration.

MALDI mass spectrometry samples were prepared by diluting catholyte and anolyte samples (~ 2 mL) in dichloromethane (~ 7 mL) and washing the organic layer with water (~ 100 mL) two times. The organic layer was then concentrated under reduced pressure. Supporting electrolyte salt needed to be removed prior to MS analysis.

^{1}H NMR samples were prepared by diluting catholyte and anolyte samples in acetone-d_6.

III. Figures

Figure S1: Discharge capacity change of $Fe(bpy)_3(BF_4)_2$ in 5 supporting electrolytes over 20 cycles.

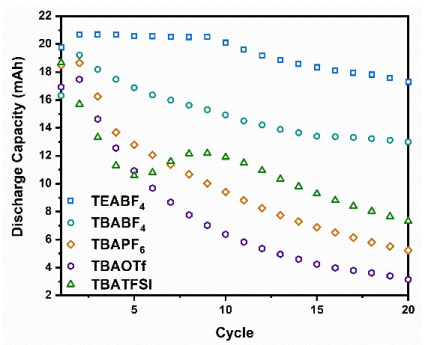

Figure S2: Post-battery cyclic voltammograms and ^{1}H NMR spectra of anolytes and catholytes from symmetric RFBs, compared to un-cycled $Fe(bpy)_3(BF_4)_2$ (10 mM), in various supporting electrolytes. Measured in the respective supporting electrolyte (0.5 M) in propylene carbonate, at 100 mV s^{-1}, using a Ag/AgCl reference electrode in 0.5 M $TBABF_4$/PC, Pt wire counter electrode, and 3 mm glassy carbon working electrode.

A. $Fe(bpy)_3(BF_4)_2$ in $TEABF_4$/PC

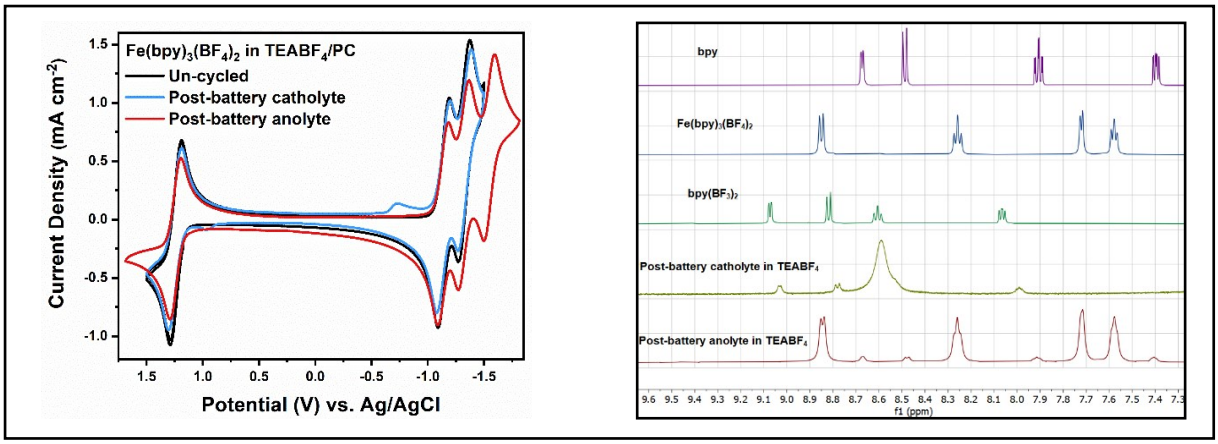

B. $Fe(bpy)_3(BF_4)_2$ in $TBABF_4$/PC

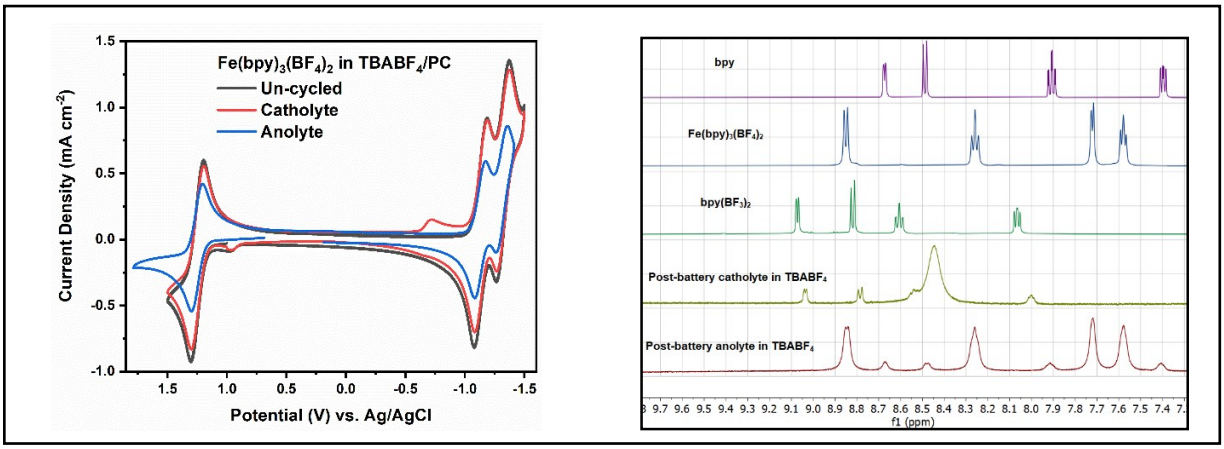

C. $Fe(bpy)_3(BF_4)_2$ in $TBABF_4$/PC

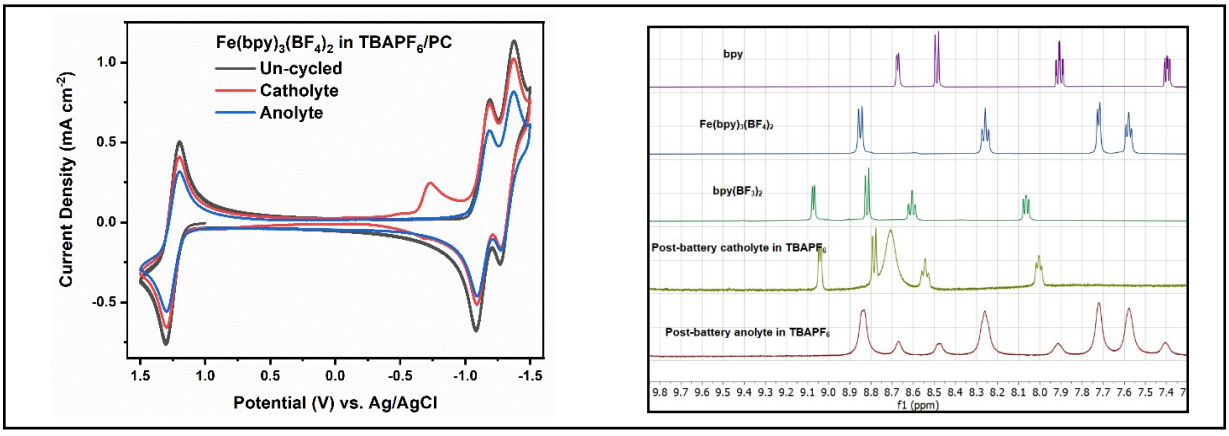

D. $Fe(bpy)_3(BF_4)_2$ in TBAOTf/PC

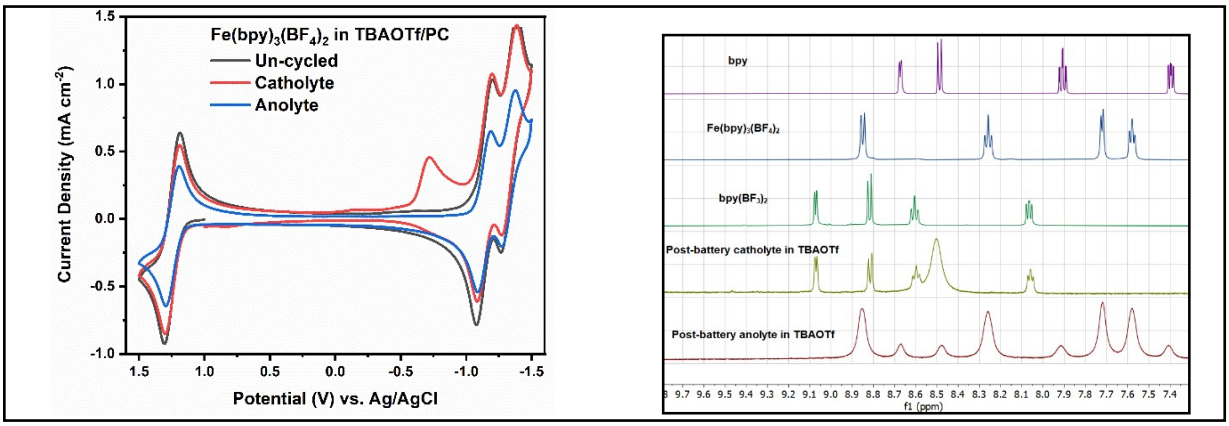

E. $Fe(bpy)_3(BF_4)_2$ in TBATFSI/PC

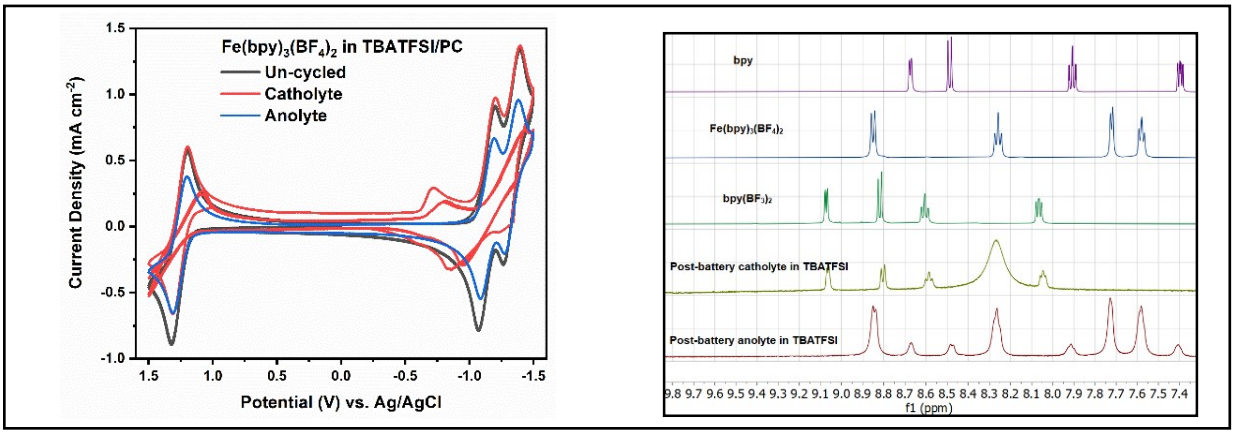

Figure S3: Un-cycled $Fe(bpy)_3(BF_4)_2$ in TBATFSI/PC (0.5 M) and post-battery catholyte before and after counteranion exchange.

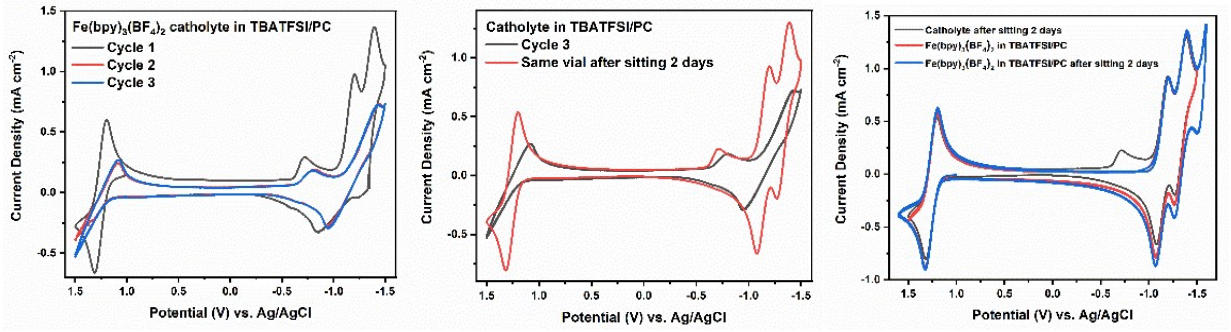

Figure S4: Absorbance spectra of each Fe bpy complex in propylene carbonate.

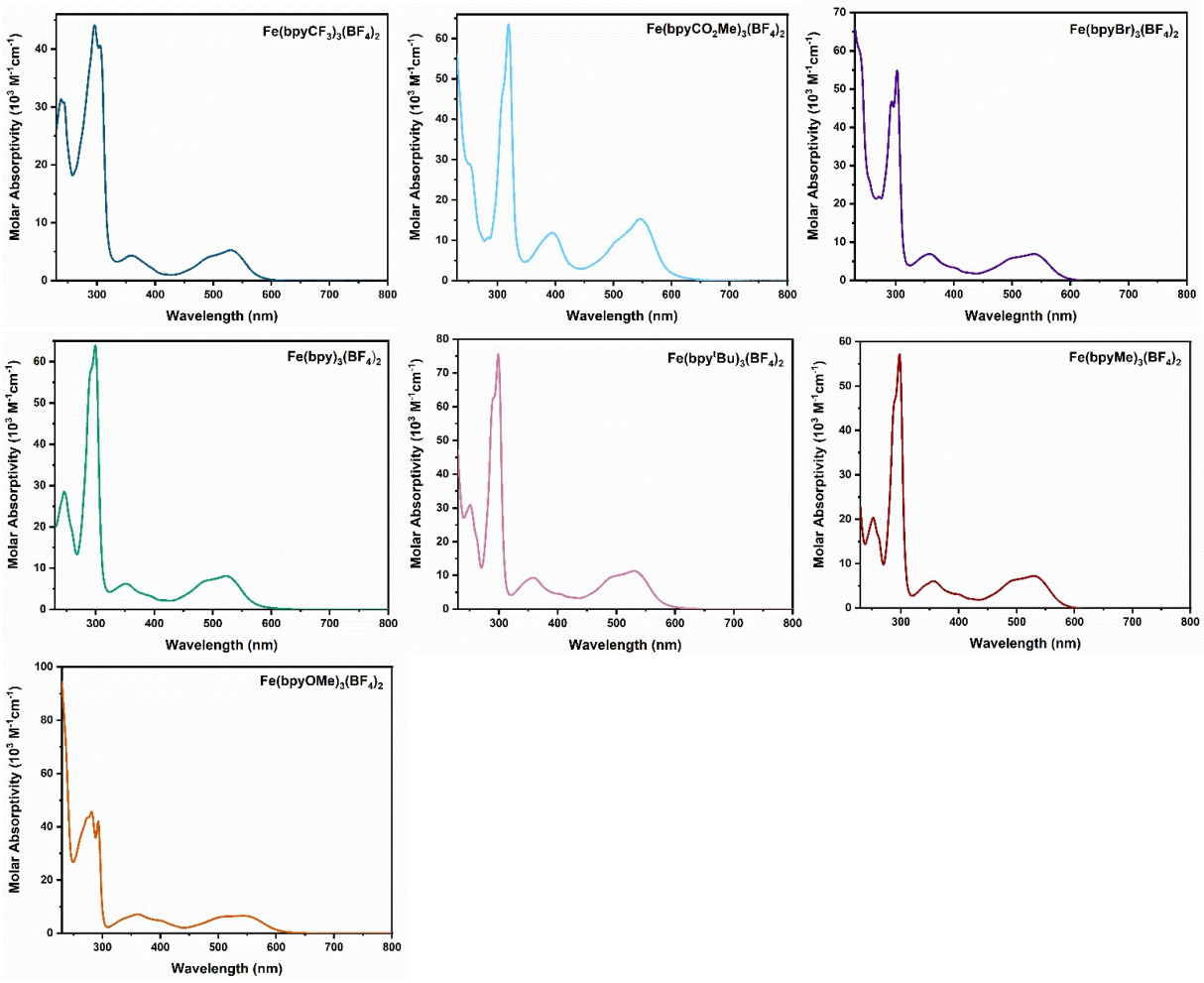

Figure S5: Scan rates and diffusion coefficients of $Fe(bpyR)_3(BF_4)_2$ (10 mM) in 0.5 M $TEABF_4$/PC, ranging from 25 to 500 mV s^{-1}, using a Ag/AgCl reference electrode in 0.5 M $TBABF_4$/PC, Pt wire counter electrode, and 3 mm glassy carbon working electrode.

A. $Fe(bpyCF_3)_3(BF_4)_2$

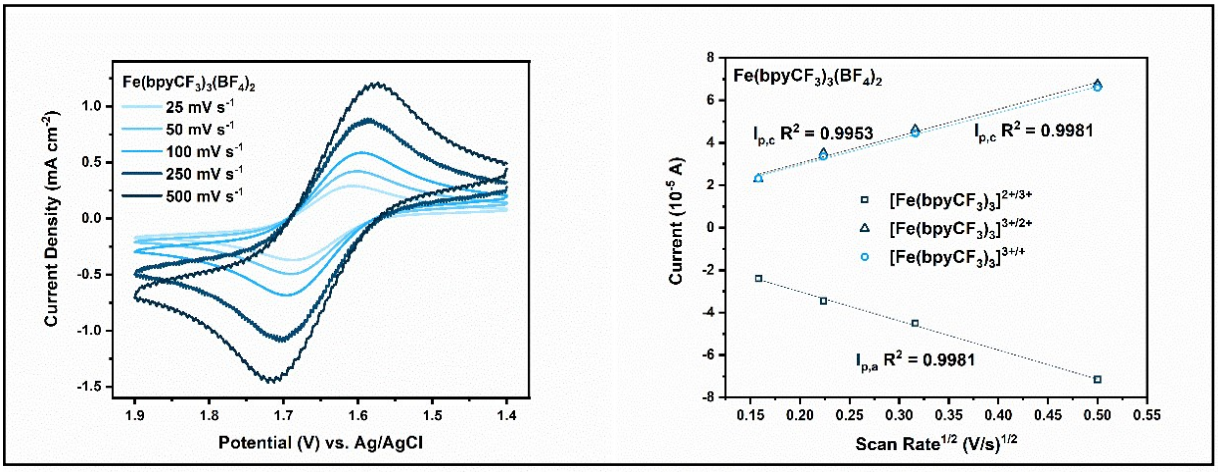

B. $Fe(bpyCO_2Me)_3(BF_4)_2$

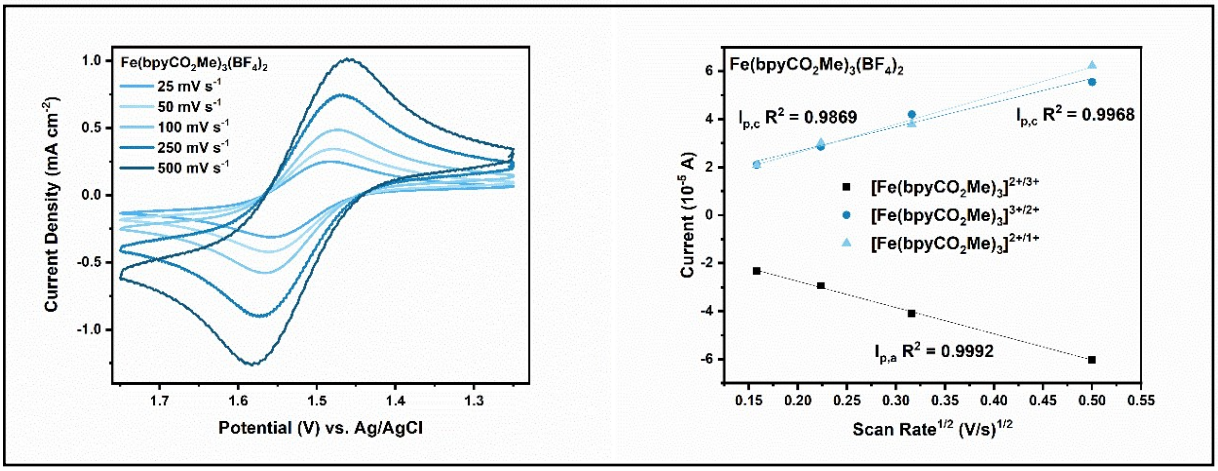

C. $Fe(bpyBr)_3(BF_4)_2$

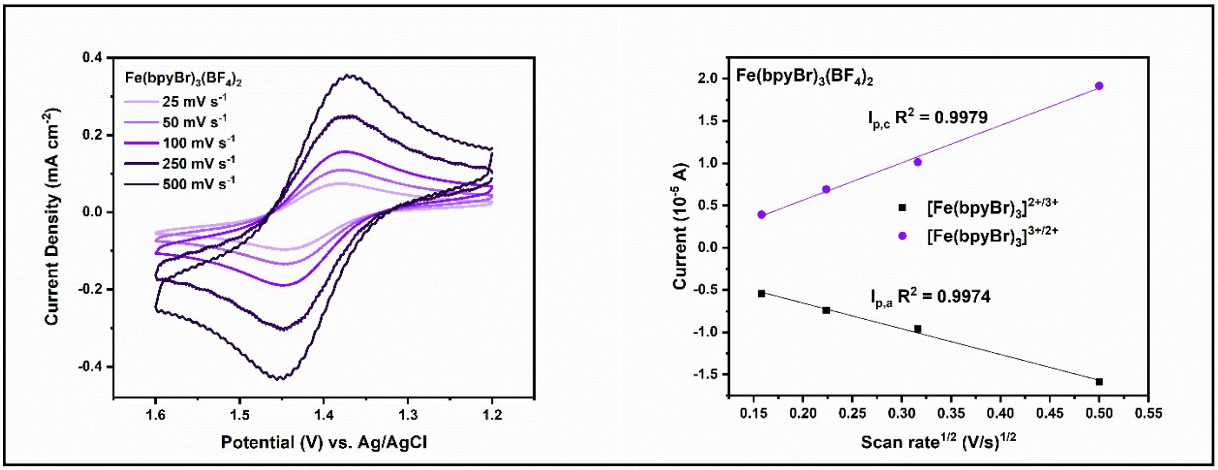

D. $Fe(bpy)_3(BF_4)_2$

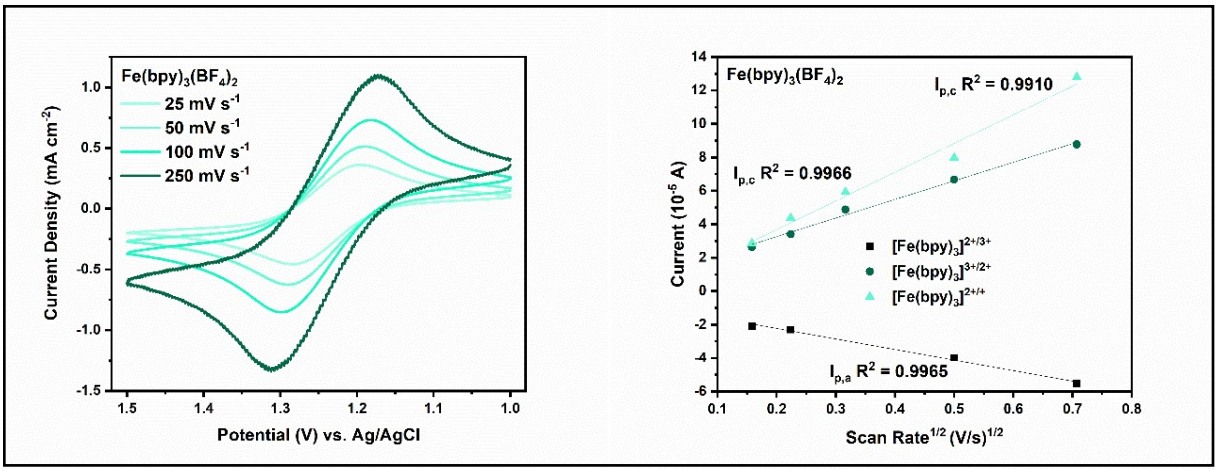

E. $Fe(bpy^tBu)_3(BF_4)_2$

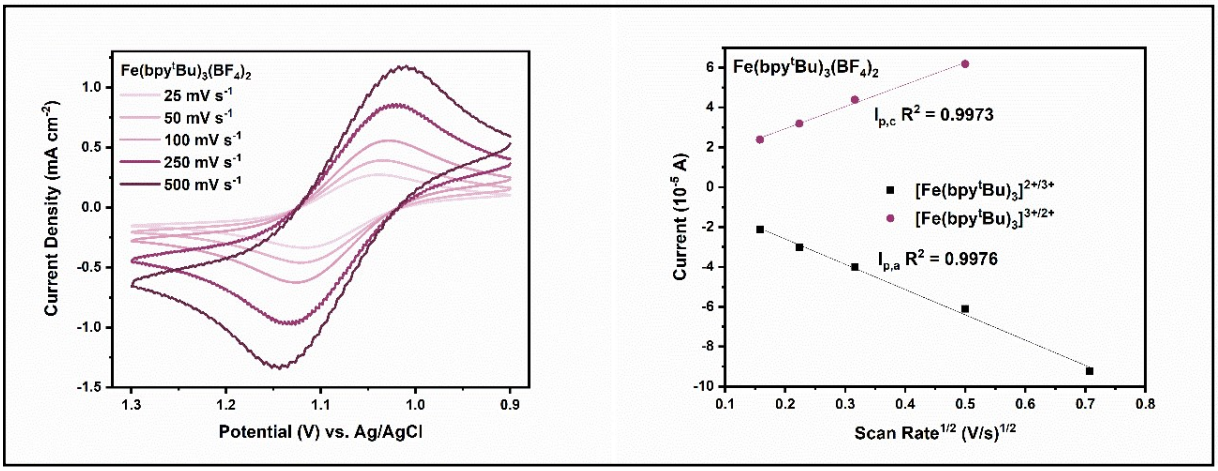

F. $Fe(bpyMe)_3(BF_4)_2$

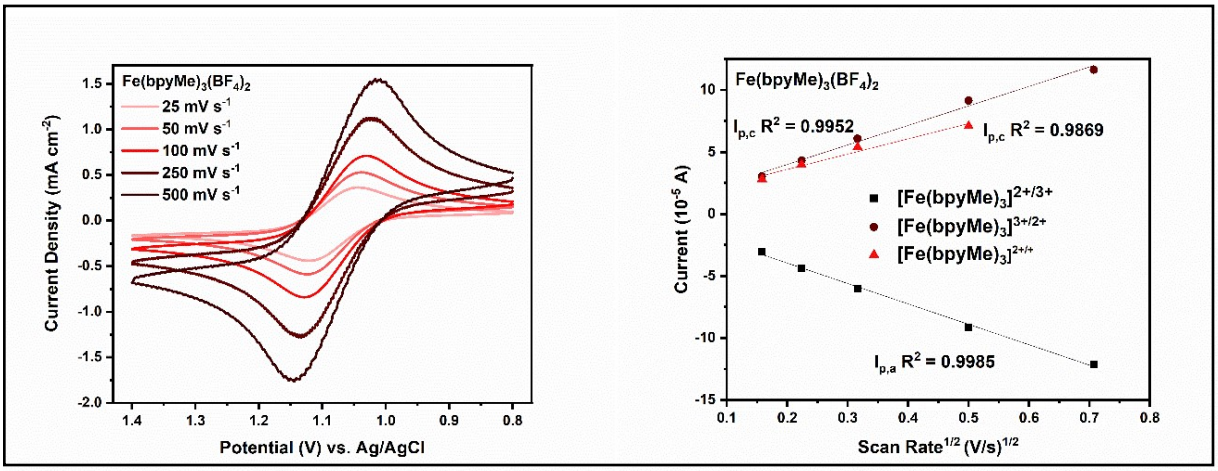

G. $Fe(bpyOMe)_3(BF_4)_2$

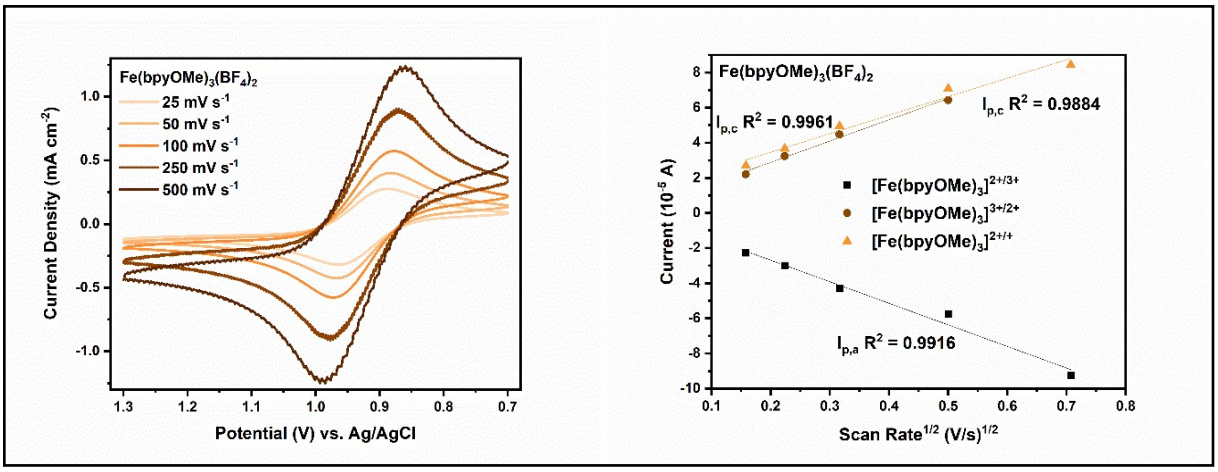

Figure S6: Electrochemical analysis of $Fe(bpyNH_2)_3(BF_4)_2$-Nafion thin film measured using a Ag/AgCl reference electrode in 0.5 M $TBABF_4$/PC, Pt wire counter electrode, and 3 mm glassy carbon working electrode. A mixture of $Fe(bpyNH_2)_3(BF_4)_2$ (25.4 mg) in 7 mL acetone, 2 mL isopropanol, and 1 mL 5 % Nafion solution was sonicated for 5 minutes and drop-casted onto a glassy carbon working electrode.

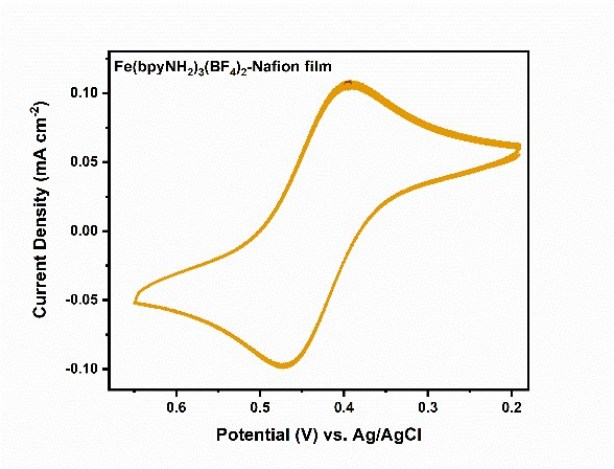

Figure S7: Post-battery cyclic voltammograms and ^1H NMR of symmetric $Fe(bpyCF_3)_3(BF_4)_2$ catholyte and anolyte.

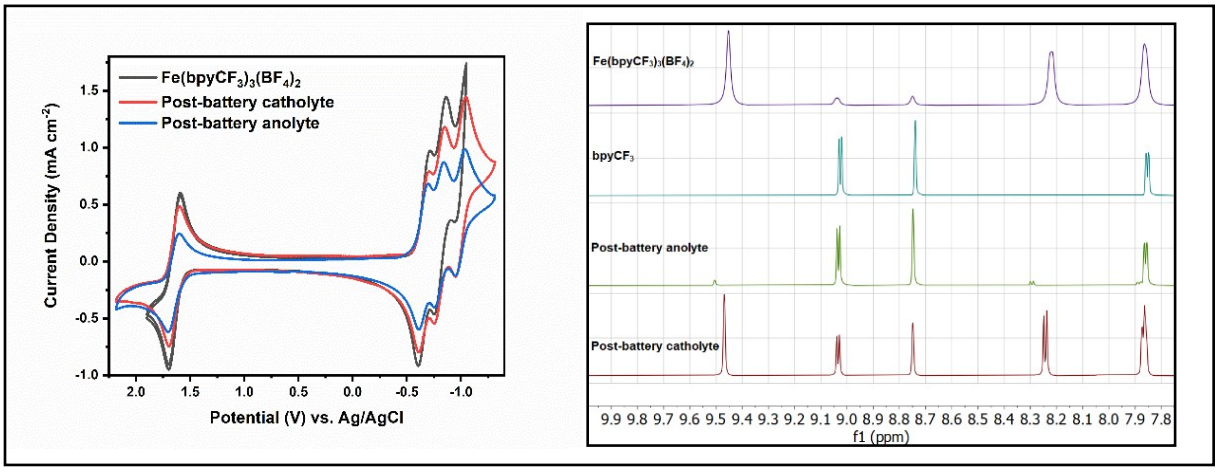

Figure S8: MALDI-MS of symmetric $Fe(bpyCF_3)_3(BF_4)_2$ catholyte. Modeled $Fe(bpyCF_3)_3$ catholyte $[M+H]^+$ (top) and detected (bottom) in low concentrations.

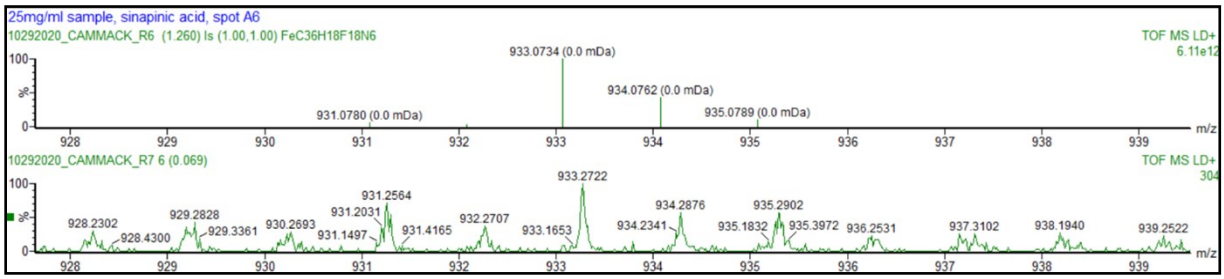

Figure S9: Post-battery cyclic voltammograms and ^1H NMR of $Fe(bpyOMe)_3(BF_4)_2$ catholyte and anolyte.

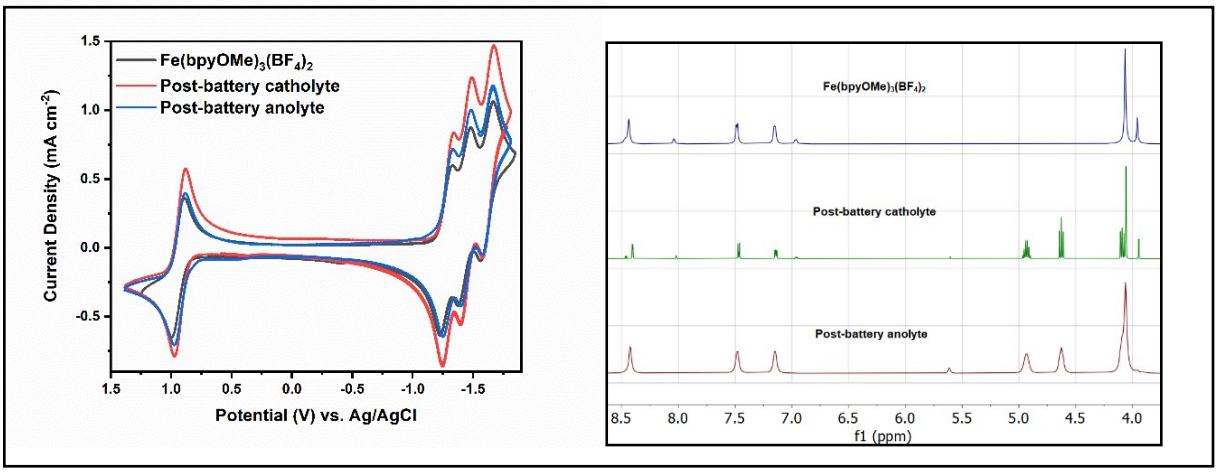

Figure S10: Post-battery cyclic voltammograms and ^{1}H NMR of Optimized catholyte and anolyte.

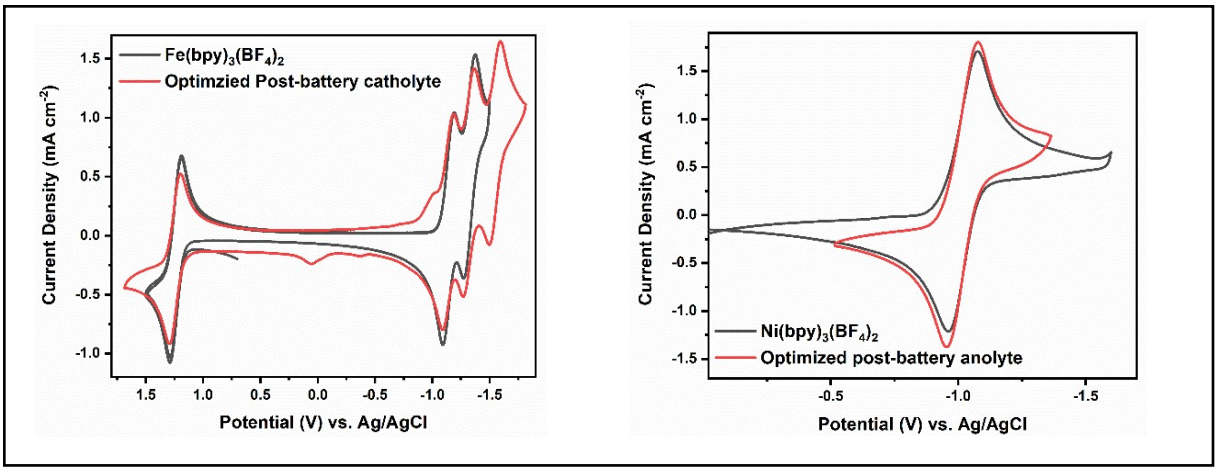

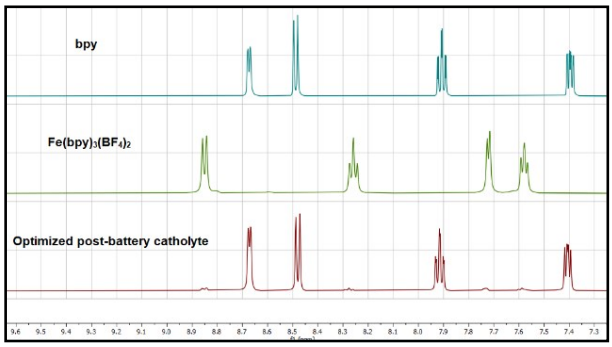

Figure S11: MALDI-MS of Optimized catholyte and anolyte.

A. Modeled $Fe(bpy)_3$ $[M+H]^+$ (top) and detected (bottom) at low concentrations in catholyte.

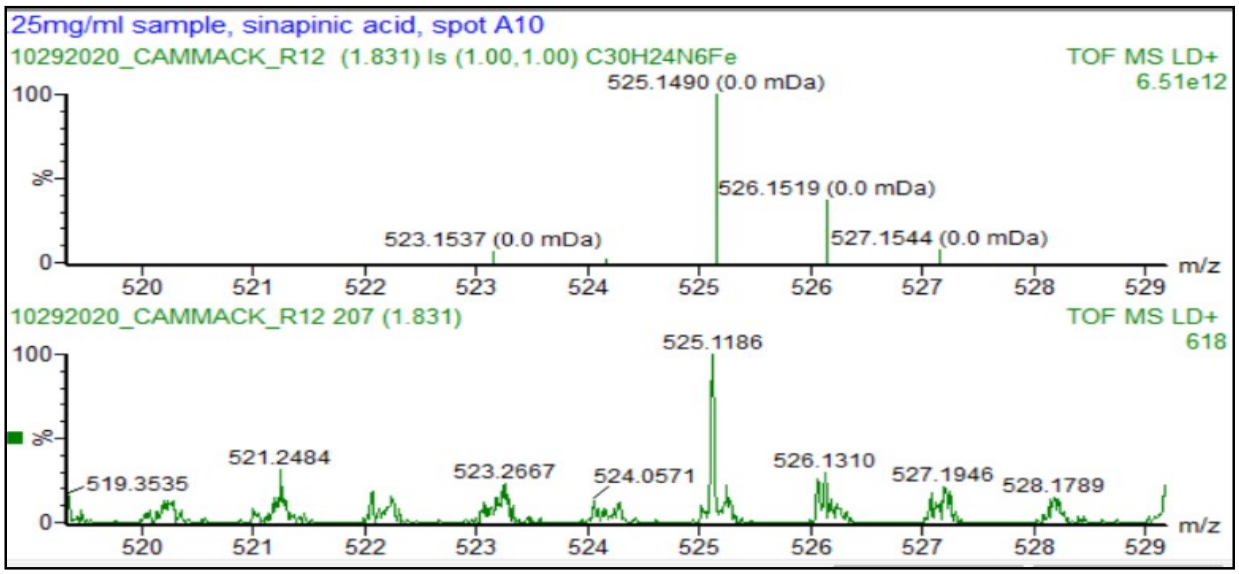

B. Modeled hydrolysis products $[M+H]^+$ (top 3), sinapinic acid reference, and observed by-products in catholyte.

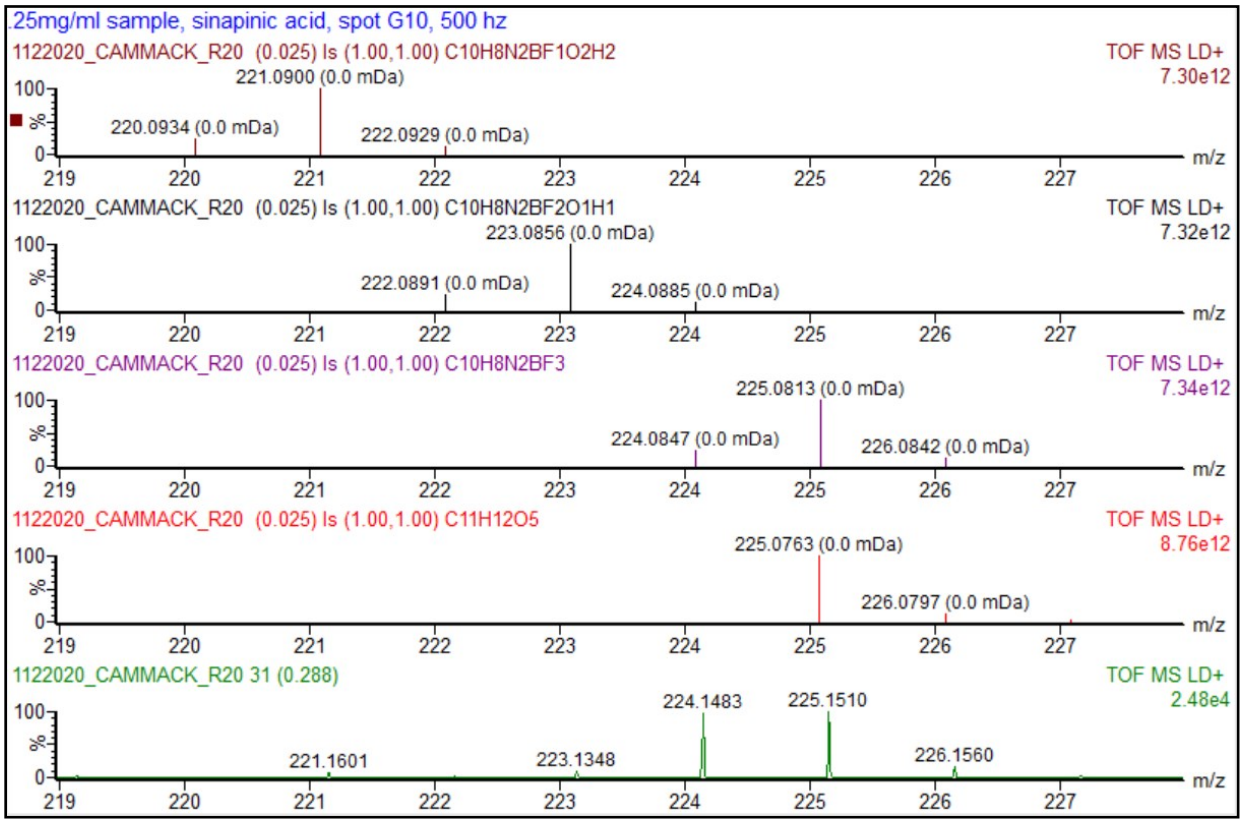

C. Modeled bpy $[M+H]^+$ (top) and detected bpy in anolyte. $Ni(bpy)_3$ could not be detected.

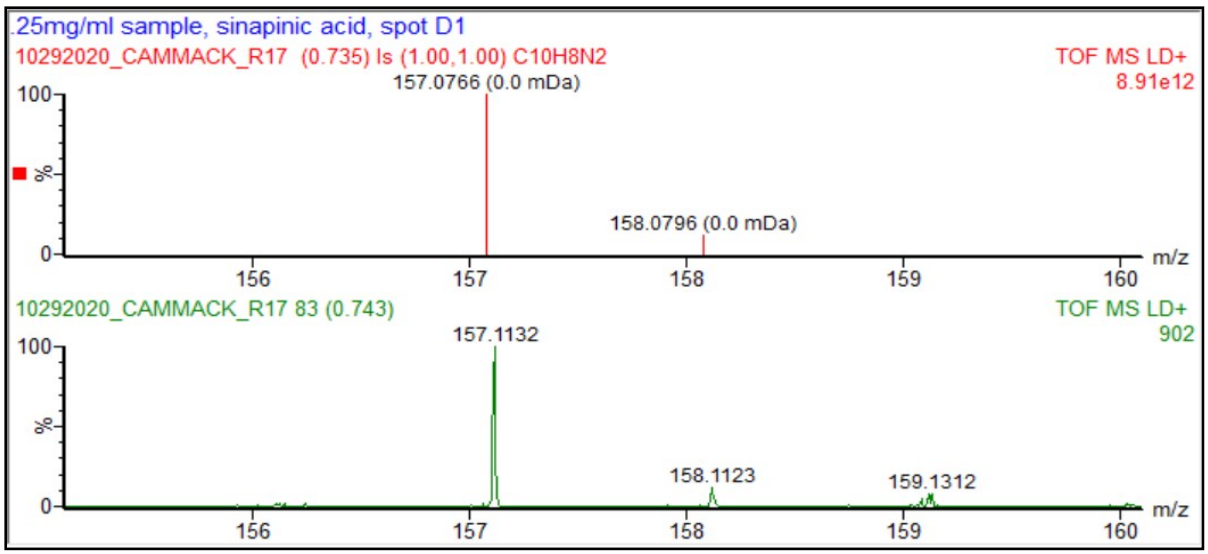

Figure S12: Post-battery cyclic voltammograms of $Fe(bpyCF_3)_3(BF_4)_2$/$FcBF_4$.

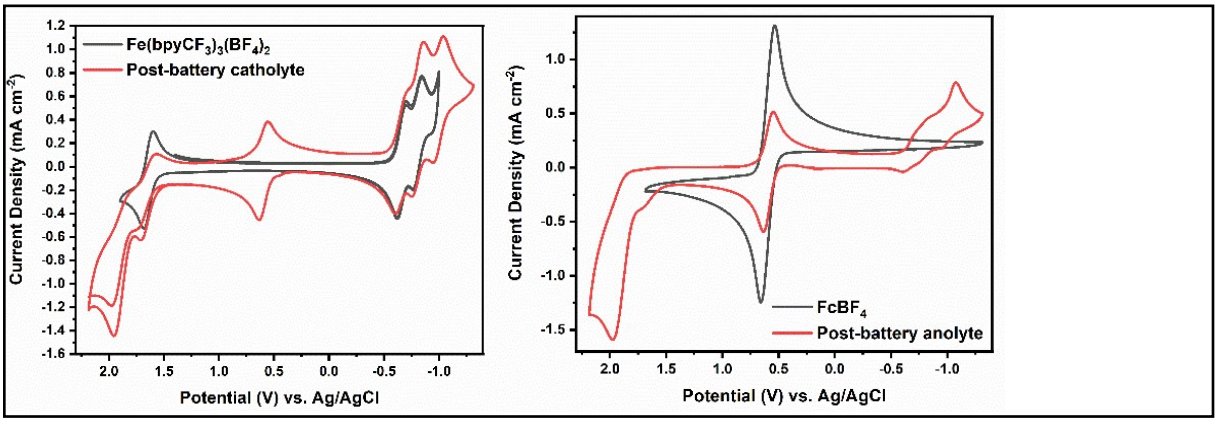

Figure S13: Post-battery cyclic voltammograms of Next Gen catholyte and anolyte.

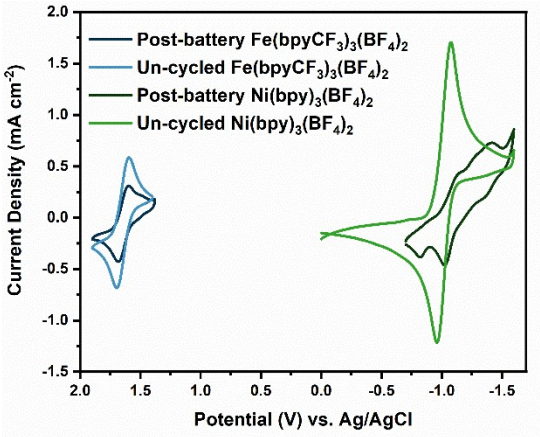

Figure S14: Post-battery MALDI-MS of Next Gen catholyte and anolyte.

A. Modeled bpy(CF_3)(CF_2(OH) (top) and detected (bottom) in catholyte.

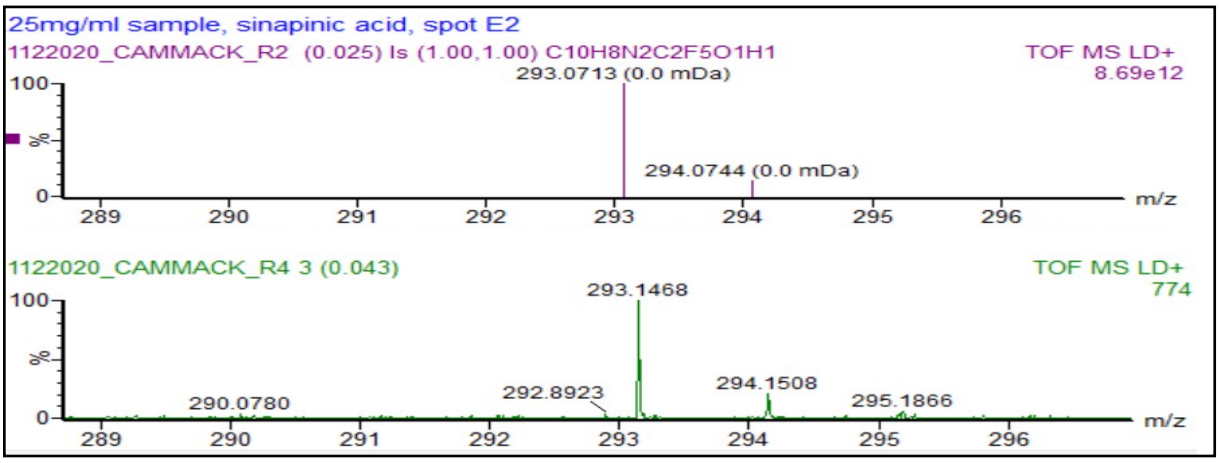

B. Modeled bpy(BF_3)$_1$ $[M+H]^+$ (top) and observed (bottom), plus additional hydrolysis products in catholyte.

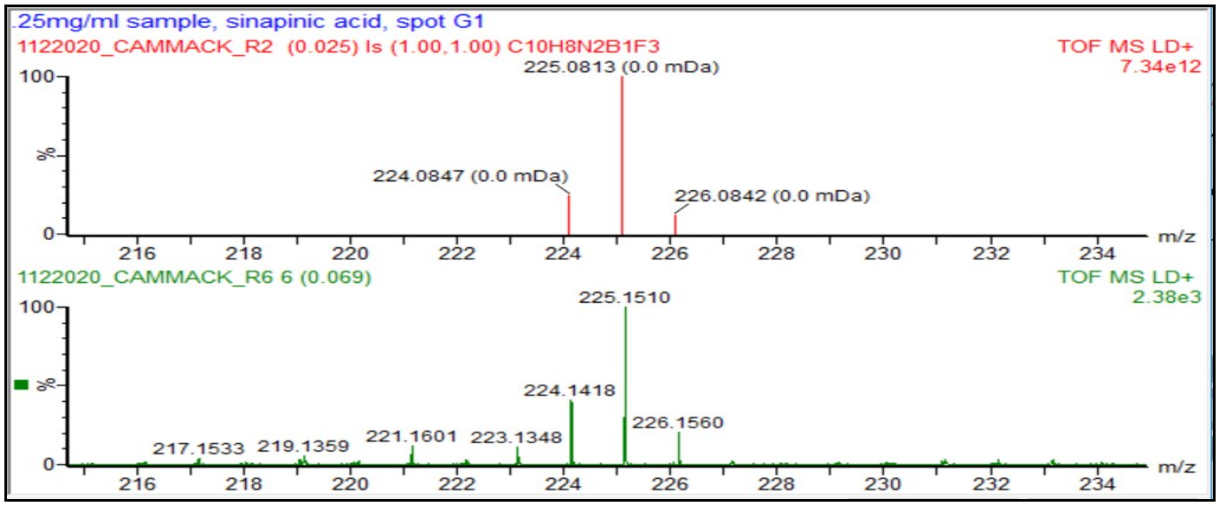

C. Modeled bpy $[M+H]^+$ (top) and observed (bottom) in anolyte.

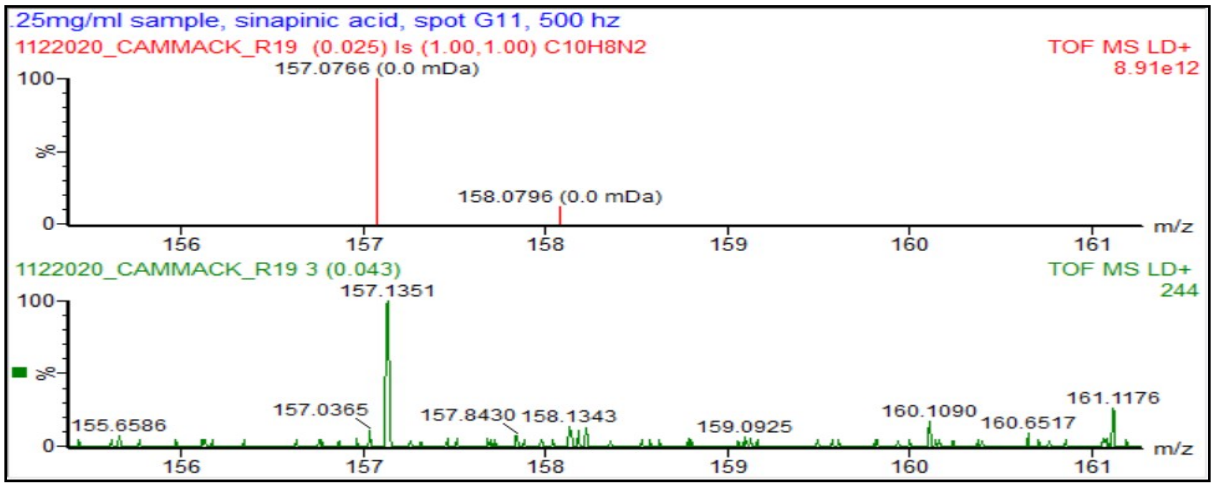

Figure S15: Post-battery cyclic voltammograms and ^{1}H NMR of Fe(bpyCF_3)$_3$(BF_4)$_2$/ Fe(bpy)$_3$(BF_4)$_2$.

A. $Fe(bpyCF_3)_3(BF_4)_2$ catholyte.

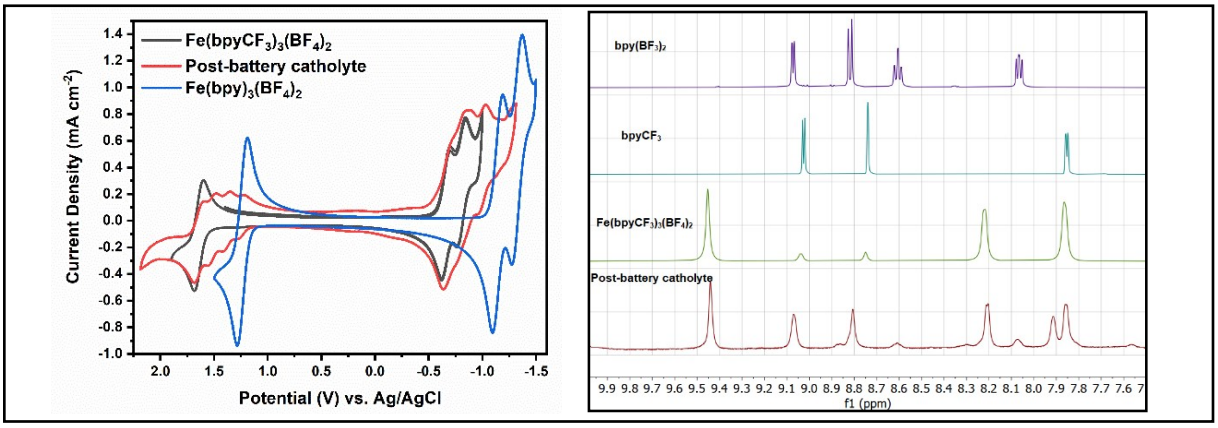

B. $Fe(bpy)_3(BF_4)_2$ anolyte.

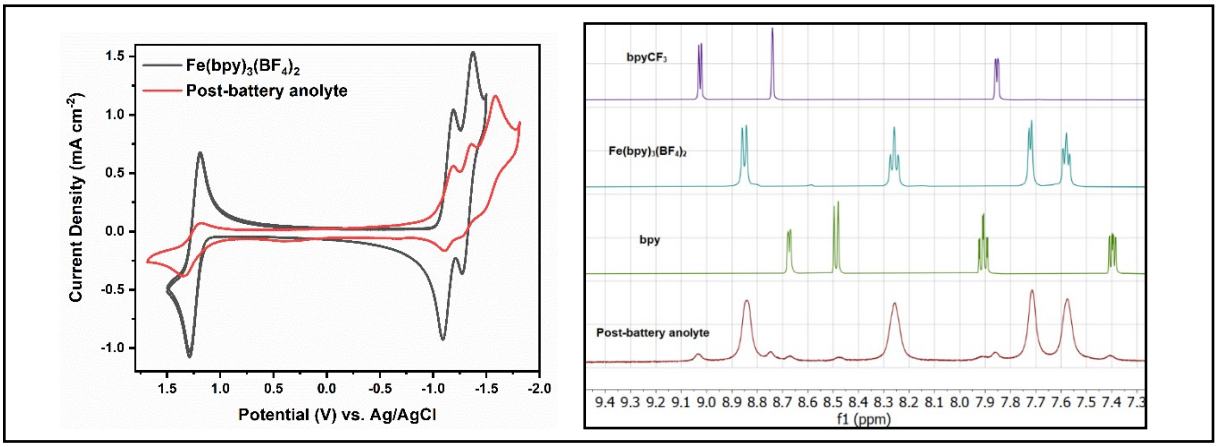

Figure S16: Standard curves of $Fe(bpy)_3(BF_4)_2$, $Fe(bpyCF_3)_3(BF_4)_2$, and $Fe(bpyOMe)_3(BF_4)_2$ in 0.5 M $TEABF_4$/PC and post-battery catholyte and anolyte absorbance measurements of symmetric $Fe(bpy)_3(BF_4)_2$, symmetric $Fe(bpyCF_3)_3(BF_4)_2$, symmetric $Fe(bpyOMe)_3(BF_4)_2$, Optimized catholyte, Next Gen catholyte, and asymmetric $Fe(bpyCF_3)_3(BF_4)_2$/$Fe(bpy)_3(BF_4)_2$ catholyte and anolyte.

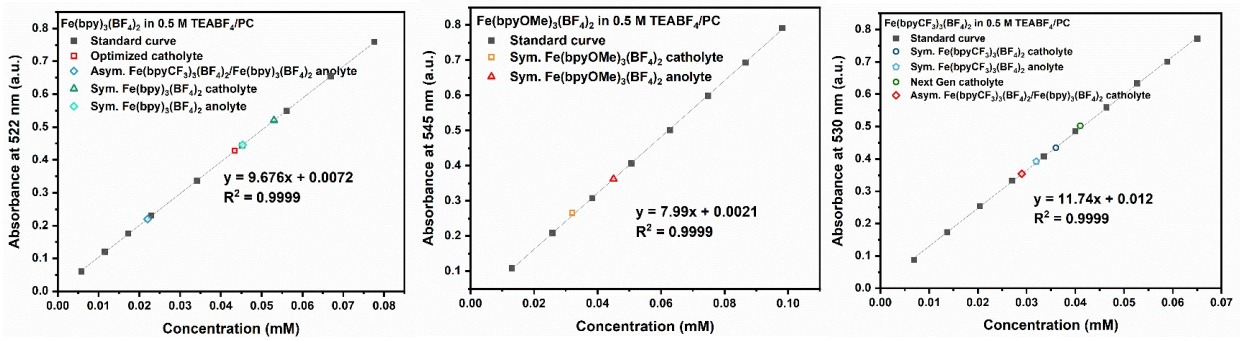

Table 1: Calculated concentrations of post-battery catholytes and anolytes determined from the standard curves in Figure S12.

Catholytes	Start: 0.2 M	Anolytes	Start: 0.2 M
Sym. $Fe(bpy)_3(BF4)2$	0.795 M	Sym. $Fe(bpy)_3(BF_4)_2$	0.679 M
Sym. $Fe(bpyCF_3)_3(BF_4)_2$	0.538 M	Sym. $Fe(bpyCF_3)_3(BF_4)_2$	0.480 M
Sym. $Fe(bpyOMe)_3(BF_4)_2$	0.495 M	Sym. $Fe(bpyOMe)_3(BF_4)_2$	0.675 M
Asym. $Fe(bpyCF_3)_3(BF_4)_2$	0.435 M	Asym. $Fe(bpy)_3(BF_4)_2$	0.330 M
Optimized	0.651 M		
Next Gen	0.630 M		

IV. References

(1) Armstrong, C. G.; Hogue, R. W.; Toghill, K. E. Characterisation of the Ferrocene/Ferrocenium Ion Redox Couple as a Model Chemistry for Non-Aqueous Redox Flow Battery Research. *J. Electroanal. Chem.* **2020**, *872*, 114241. https://doi.org/10.1016/j.jelechem.2020.114241.